4
Relaxations on the Nanoscale: An Atomistic View by Numerical Simulations

Christine Mottet

Atomic structure of materials reveals usually significant deviations compared to perfect periodic bulk crystals. Condensed matter is made of defects, some of them being essential for physical properties such as doping in semiconductors (extrinsic defects), other ones such as vacancies, dislocations, or grain boundaries are key elements for mechanical properties of materials, especially in the plastic domain. Defects come from the elaboration mode and thermal treatment of the materials. When the dimensions of the system decrease, the surface and interfaces become important, and the structure can be modified in the vicinity of these extended defects. The cut bonds at the surface or the epitaxial relation at the interface may not only induce stress and strain in the neighborhood of the defect but also possible reorganization, both atomically and chemically in case of alloys. Such structural modifications have a stronger impact when the size of the system is reduced at the nanoscale, as in clusters or nanoparticles.

Nowadays, experimental improvements make it possible to elaborate and characterize nanomaterials. In parallel, theory and especially atomistic models based on numerical simulations (semiempirical potentials or *ab initio* methods in the density functional theory, DFT) made significant progress in describing the relaxation processes leading to energy optimization. As a consequence, we know that such defects are associated with lattice deformations and reconstructions, or even chemical rearrangements minimizing the total energy of the system but not necessarily its stress. In case of pure systems such as surface or clusters, we show that energy minimization can lead to relatively high-stressed systems as in the case of the (1×2) reconstructed metallic surfaces or in the case of small icosahedral clusters with high compression in their core. In contrast, in alloy surfaces and nanoalloys, we usually find that the release of the stress coming from the size mismatch between the two components is a driving force for stabilization of the system.

This chapter will develop different aspects of the atomistic approach by numerical simulations of relaxations at the nanoscale in five sections. After a short introduction, the theoretical models and basic numerical simulations will be described in Section 4.2. Then, the relaxations in surfaces and interfaces (surface reconstructions, alloy surfaces, and heteroepitaxial thin films) will be discussed in

Mechanical Stress on the Nanoscale: Simulation, Material Systems and Characterization Techniques, First Edition. Edited by Margrit Hanbücken, Pierre Müller, and Ralf B. Wehrspohn.

Section 4.3, before dealing with the relaxations in nanoclusters (unsupported pure clusters, supported clusters, and nanoalloys) in Section 4.4. The last section will stand for conclusions.

4.1 Introduction

In linear elasticity theory, the stress and strain relation described under the form of the Hooke's law is based on the continuum concept for the matter that has been well represented using a tensorial notation, as introduced by the French mathematician Augustin Louis Cauchy (1789–1857). It has been able to describe most of the elastic deformation both in macroscopic and in microscopic systems. However, going to smaller and smaller systems sizes up to the nanometer scale, it becomes more evident that the description at the atomic level is more relevant. In particular, when the atomic structure is sensibly modified compared to the bulk periodic structure, we can expect that in the vicinity of the perturbations, the elastic theory fails. In the following, we will show, however, that the linear elasticity theory reproduces well the strain at a certain distance of the stressed region but not necessarily exactly in the center of the defect. So we find that the two aspects, continuum theory and atomistic description, are essentially complementary.

The concept of "relaxation" in physics is not exactly the same as in current life. In the occidental way of life, the relaxation represents a process or state with the aim of recreation through leisure activities or idling, the opposite of stress or tension. In the oriental civilization, the relaxation could be associated with meditation as taught by Zen masters. In physics, the relaxation is a response to external (or internal) stress (or strain). It implies both the time-dependent process of this mechanical perturbation that we will rather call dynamical relaxation, involving the physical and atomistic mechanism the system uses to reach its relaxed state, and the final relaxed state that we will essentially consider here. When a load is applied to a system as in the traction experiment, the system is strained because of the external stress and the atomic positions may change. We will not consider the way they will move (the dynamics) but their final configuration in the final relaxed state, whatever the way this state has been reached. Even if a system is free of external stress, this does not mean it is free of strain. Indeed, because of defects such as surfaces, interfaces, grain boundaries, or dislocations, a system can be strained by itself, without any load applied. In such cases, the system presents some deviations compared to the bulk periodic structure. This will be described at the atomic level by numerical simulations. The strain pattern is controlled by the energy minimization. The system optimizes its energy by moving some of its atoms (optimizing the bond length as a function of the local environment and in particular the number of near neighbors) and by exchanging atoms of different species in the case of alloys. For example, some surfaces are reconstructed in order to compensate their lack of bonds, such as the famous (7×7) reconstruction of the Si(111) surface [1] or the Au(111) surface reconstruction [2].

4.2
Theoretical Models and Numerical Simulations

Modelization of the energy of the system is the crucial point in order to perform realistic and reliable simulations. There are different approaches with different degrees of accuracy corresponding to different levels of description of the electronic structure from the first-principles methods using the density functional theory to semiempirical potentials fitted to experimental properties or, eventually, on *ab initio* calculations if experimental data do not exist. In parallel to the energetic model, we will illustrate the basic statistical thermodynamic methods in numerical simulations, that is, molecular dynamics and Monte Carlo simulations, to describe the equilibrium configuration corresponding to the minimum energy state in the fundamental state (at OK) or at finite temperature.

4.2.1
Energetic Models

According to the first principles, the Schrödinger equation for a system of N electrons moving in the electrostatic field created by M atomic nuclei is written as

$$H\Omega = E\Omega \tag{4.1}$$

where H is the Hamiltonian operator, E is the energy, and $\Omega(r_1, \ldots, r_N, R_1, \ldots, R_M)$ is the wave function, which depends on the electrons' r_i and nuclei R_i positions. The Born–Oppenheimer (adiabatic) approximation consists in separating the movement of the electrons from those of the nuclei, knowing the electron mass is much less than the nuclei one. Thus, the electrons in their fundamental state follow the nuclei in such a way that Ω can be written as

$$\Omega = \Phi(R_1, \ldots, R_M)\Psi(r_1, \ldots, r_N) \tag{4.2}$$

and the wave function of the electrons comes from the resolution of the Schrödinger equation in the field of the nuclei

$$H_e\Psi(r) = E_e\Psi(r) \tag{4.3}$$

where the electrons' Hamiltonian H_e is the sum of three contributions

$$H_e = T + V + U \tag{4.4}$$

with the kinetic energy T

$$T = \frac{1}{2}\sum \nabla\Psi^*(r)\nabla\Psi(r)\mathrm{d}r \tag{4.5}$$

the potential V that represents the interaction of the electrons in the potential of the nuclei

$$V(r) = \sum \nu(r)\Psi^*(r)\Psi(r)\mathrm{d}r \tag{4.6}$$

and the Coulomb interaction of the electrons between each other U

$$U = \frac{1}{2}\sum \frac{1}{|r-r'|}\Psi^*(r)\Psi^*(r')\Psi(r)\Psi(r')\mathrm{d}r\,\mathrm{d}r' \tag{4.7}$$

The coupling of N electrons by the Coulomb repulsion and the exchange interaction coming from the Pauli exclusion lead to a complex system that is essentially impossible to resolve without approximation. There are two kinds of approximations: the Hartree–Fock method, where the N electrons' problem is transformed into N coupled equations with one electron in an effective potential via a Slater determinant, and the density functional theory from the Hohenberg and Kohn theorem (1964) [3]. We will briefly describe the second method, the most used at present.

According to the remarkable theorem of Hohenberg and Kohn [3], the energy of a free electron gas in interaction in an external potential $v(r)$ is a functional $F[n(r)]$ of their density $n(r)$, with the minimal value corresponding to the fundamental state. The functional $F[n(r)]$, independent of $v(r)$, is defined, according to Kohn and Sham [4], as

$$F[n(r)] = T_s[n(r)] + \frac{1}{2}\iint \frac{n(r)n(r')}{r-r'}\mathrm{d}r\,\mathrm{d}r' + E_{\mathrm{xc}}[n(r)] \tag{4.8}$$

where $T_s[n(r)]$ is the kinetic energy of an electron gas without interaction with density $n(r)$, the second term is that of Hartree (mean field approximation) to treat the Coulomb interaction, and the last term is that of exchange and correlation that takes into account all that has been neglected before. The variational problem of the Schrödinger equation can be solved as a system of one electron in an effective potential

$$\left(-\frac{1}{2}\nabla^2 + V_{\mathrm{eff}}(r)\right)\psi_i(r) = \varepsilon_i\psi_i(r) \tag{4.9}$$

with the effective potential

$$V_{\mathrm{eff}} = v(r) + \int \frac{n(r')}{|r-r'|}\mathrm{d}r' + V_{\mathrm{xc}}(n(r)) \tag{11}$$

where $V_{\mathrm{xc}}(n(r))$ is the exchange and correlation contribution to the potential. This system of Kohn–Sham equations can be solved in an iterative way: starting with a density $n(r)$ using monoelectronic functions $\psi_i(r)$ on a given set of wave functions, we calculate the effective associated potential and we solve the Kohn–Sham equations by diagonalization of the matrix. The eigenvectors give the new wavefunctions $\psi_i(r)$ and thus the new density $n(r)$. The energy is integrated numerically over all the k vectors of the Brillouin zone and the self-consistent process is followed up to the convergence of the energy.

The two principal exchange and correlation functionals, widely used, are the local density approximation (LDA), which corresponds approximately to a homogeneous electron gas with a sum of local contributions. It is quite correct when the variations

in the density are weak. The second one is the generalized gradient approximation (GGA), which is better in the case where the density can fluctuate as in the vicinity of defects (surfaces) or open systems (molecules).

Anyway, *ab initio* methods in general are time consuming and can be used efficiently only on very small systems (less than hundreds of atoms) or low symmetry, and using a quite poor statistic or a quite short time of dynamics. For larger-scale systems, always keeping the atomistic description, we can use semiempirical potentials and in particular many-body potentials for metallic systems.

We will describe briefly the tight binding second moment approximation (TB-SMA) model. In this model, the main features of the cohesion of transition metals are well reproduced by the bandwidth of the density of states [5], which we approximate by a rectangular shape with the same width [6]. By this way, the band energy term at site i can be written simply

$$E_i^b = -\sqrt{\xi^2 \sum_j \mathrm{e}^{-2q(r_{ij}/r_0-1)}} \tag{4.11}$$

where ξ is an effective hopping integral, r_{ij} is the distance between the atoms at sites i and j, r_0 is the first-neighbor distance in the metal. The summation goes over all the neighbors up to the cutoff distance r_c. The total energy of a system of N atoms is written as a sum of the band energy term (attractive part) and a repulsive term of the Born–Mayer type

$$E_i^r = A \sum_j \mathrm{e}^{-p(r_{ij}/r_0-1)} \tag{4.12}$$

where the parameters (ξ, A, q, p) are fitted to different experimental values: bulk cohesive energy (ε_B), lattice parameter (a), and elastic constants (B, C_{44}, C') [7] of the metal. This many-body potential is comparable to other well-known methods such as the embedded atom method (EAM) [8] or the corrected effective medium (CEM) theory [9, 10]. Although not as precise as the *ab initio* methods [11, 12], the TB-SMA approach describes quite correctly, at least qualitatively if not quantitatively, the relaxation and/or some of the possible reconstructions of the low-index surfaces [13].

4.2.2
Numerical Simulations

The archetypal methods used in numerical atomistic simulations are essentially of two kinds, the molecular dynamics (MD) and the Monte Carlo (MC) simulations, which are well described by Frenkel and Smit [14], and Allen and Tildesley [15]. A lot of other methods have been developed, mainly to overcome the time limitation of the MD simulation to describe real time-dependent processes. The idea of these methods (accelerated dynamics [16], ART [17], NEB [18], or dimer method [19]) is to accelerate the dynamics by the study of the whole energy landscape [20] and in particular the determination of the saddle points in order to cross the energy barriers more efficiently and in an acceptable simulation timescale. We will not describe all these

more sophisticated methods but give here only the essential elements to give a first insight into the basic atomistic simulation methods (MD and MC simulations). Moreover, in the large majority of the examples given hereafter, we will concentrate on the final relaxed states, obtained from a local relaxation of the atomic positions starting from a configuration that is near the final one. This does not require to perform a full dynamical relaxation process because we are less interested by the relaxation mechanism than by the description of the final relaxed state. In the case of the nanoalloys, some of the atomic structures are coming from global optimization methods [21] that are efficient methods to find the lowest energy structure (global minimum) in the whole energy landscape [20].

In MD simulations, the Newton equations

$$F_i(t) = m\frac{d^2 r_i(t)}{\mathrm{d}t^2} = -\frac{\mathrm{d}E_{\mathrm{pot}}}{\mathrm{d}r_{ij}} \tag{4.13}$$

give, by integration using the Verlet algorithm [22], the atomic positions $r_i(t)$

$$r_i(t+\mathrm{d}t) = 2r_i(t) - r_i(t-\mathrm{d}t) + \frac{F_i(t)}{m}\mathrm{d}t^2 + \varepsilon(\mathrm{d}t^4) \tag{4.14}$$

and the atomic velocities

$$v_i(t) = \frac{r_i(t+\mathrm{d}t) - r_i(t-\mathrm{d}t)}{2\mathrm{d}t} \tag{4.15}$$

We can deduce from the velocities, the kinetic energy

$$E_{\mathrm{cin}} = \sum_{i=1}^{N} \frac{1}{2} m_i v_i(t)^2 \tag{4.16}$$

and the temperature T of the system thanks to the equipartition principle

$$\frac{3}{2}NkT = \sum_{i=1}^{N} \frac{1}{2} m_i v_i(t)^2 \tag{4.17}$$

where k is the Boltzmann constant. We can let the system evolve in the microcanonical ensemble keeping constant the total energy (kinetic + potential), the number of particles, and the volume of the system. Looking for the equilibrium state, we can perform quenched MD in order to search for the potential energy minimum: the velocity of an atom i is set to zero each time $F_i v_i < 0$. Equilibrium state at finite temperature can be reached if the MD simulation is sufficiently long in time in order to explore the phase space according to the ergodicity principle.

The MC simulations are the other great family of statistical simulation methods to determine the equilibrium state of one system in terms of atomic structure and chemical arrangement. Based on the Metropolis algorithm [23], it makes successive random trials modifying the atomic configuration of the system following a Markov

chain. The probability of acceptance of a given configuration is defined by a Boltzmann canonical distribution

$$\mathcal{P}(\mathcal{C}) \propto \mathrm{e}^{-E_C/kt} \tag{4.18}$$

and the probability of transition from one initial configuration $\mathcal{C}$ to a final one $\mathcal{C}'$ is defined by

$$W(\mathcal{C} \to \mathcal{C}') = \min\left\{1, \frac{\mathcal{P}(\mathcal{C}')}{\mathcal{P}(\mathcal{C})}\right\} = \min\left\{1, \mathrm{e}^{-(E_{C'} - E_C)/kT}\right\} \tag{4.19}$$

which means that the new configuration $\mathcal{C}'$ is accepted if its energy is lower than the energy of the initial configuration. If its energy is higher, the new configuration is accepted with the probability $\mathrm{e}^{-\Delta E/kT}$. Performing average of the energy over a large quantity of sampled configurations allows to characterize the equilibrium state of the system.

4.2.3 Definitions of Physical Quantities

The pertinent physical quantities used in order to describe the state of the system are essentially the defect energies extended to surfaces, interfaces, adatoms, vacancies or impurities, the surface stress, and the local pressure or stress on an atomic site.

The defect energy (surface, interface, and adsorption) is defined by the cost in energy of the system with the defect in the final state compared to the equivalent system without defect in the initial state, normalized by the number of atoms concerned with this kind of defect (N_{norm}). The initial and final states are represented schematically in Figure 4.1. The defect energy is written as

$$E_{\mathrm{defect}} = \frac{E_{\mathrm{final}} - E_{\mathrm{initial}}}{N_{\mathrm{norm}}} \tag{4.20}$$

The term "equivalent" means notably that we keep the same number of atoms and the same nature of atoms in the final and the initial state.

In that way, the *surface energy* is defined by the cost in energy to separate a bulk in two pieces creating a surface on each side. It is given by

$$\gamma = \frac{E_{\mathrm{slab}} - NE_{\mathrm{coh}}}{2N_{\mathrm{surf}}} \tag{4.21}$$

where E_{slab} is the energy of a system of N atoms with periodic conditions in two directions and no periodic condition in the third direction (see Figure 4.2). The slab is constituted of p layers of N_{surf} atoms on each, which leads to two surfaces of N_{surf} atoms. E_{coh} is the cohesion energy.

The *interface energy* writes

$$\beta = \frac{E_{\mathrm{slab}} - N^{\mathrm{A}}E^{\mathrm{A}}_{\mathrm{coh}} - N^{\mathrm{B}}E^{\mathrm{B}}_{\mathrm{coh}}}{N^{\mathrm{A}}_{\mathrm{surf}} + N^{\mathrm{B}}_{\mathrm{surf}}} \tag{4.22}$$

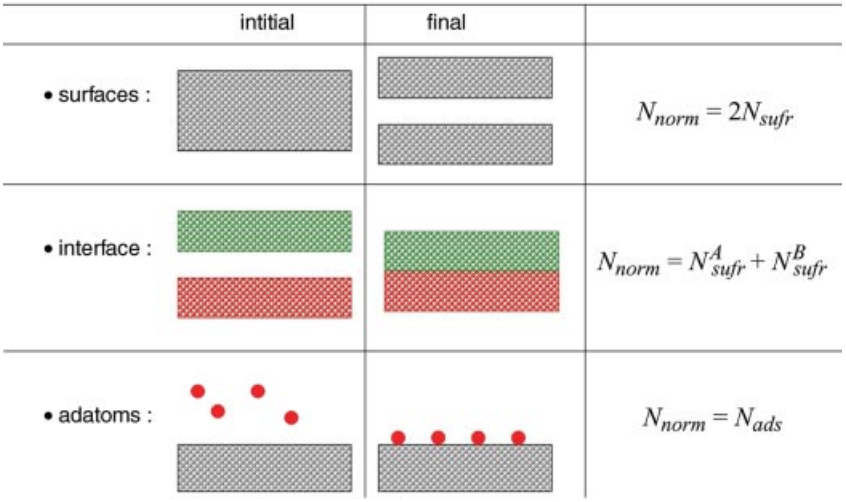

Figure 4.1 Schematic representation of the creation of surfaces, interface, and adatoms adsorption on a surface in final state compared to an equivalent system in initial state. N_{norm} gives the relevant number of atoms to normalize the defect energy.

where $E^{\text{A}}_{\text{coh}}$ and $E^{\text{B}}_{\text{coh}}$ are the cohesion energies of the two materials and N^{A} ($N^{\text{A}}_{\text{surf}}$) and N^{B} ($N^{\text{B}}_{\text{surf}}$) are the number of A or B atoms in total (or at the surface).

The *adhesion energy* is slightly different from the interface energy as the initial state is composed of two slabs of A and B with their respective surfaces. Then, it is written as

$$W = \frac{E_{\text{slab}} - E^{\text{A}}_{\text{slab}} - E^{\text{B}}_{\text{slab}}}{N^{\text{A}}_{\text{surf}} + N^{\text{B}}_{\text{surf}}} \tag{4.23}$$

The *adsorption energy* of N_{ads} adatoms, for a coverage $\theta = N_{\text{ads}}/N_{\text{surf}}$, is written as

$$E_{\text{ads}} = \frac{E^{\theta}_{\text{slab}} - E^{\theta=0}_{\text{slab}}}{N_{\text{ads}}} - \mu N_{\text{ads}} \tag{4.24}$$

where μ is the atomic potential (energy in the gas phase).

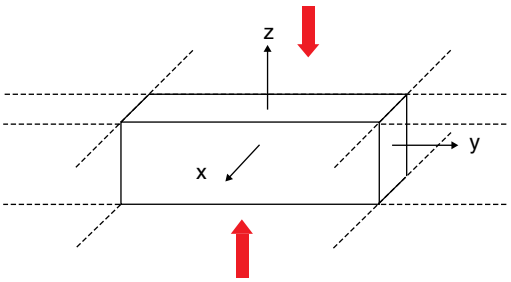

Figure 4.2 Schematic view of a slab used in numerical simulation to represent a surface (in fact, two surfaces).

Then, we can also determine the *vacancy energy* in a system of N atoms:

$$E_v = E_{\text{slab}}^{(N-1)} - \frac{(N-1)}{N} E_{\text{slab}}^{(N)} \tag{4.25}$$

And finally the *solution energy* of an atom B in a matrix of A is written as

$$E_{\text{sol}}^{\text{A(B)}} = E_{\text{slab}}^{\text{A(B)}} + \mu_{\text{A}} - E_{\text{slab}}^{\text{A}} - \mu_{\text{B}} \tag{4.26}$$

where the initial state is a slab of A and one atom of B and the final state, the same slab where one A atom has been replaced by a B atom and the A atom in gas phase.

The *surface stress* is a quantity related to the stress tensor in bulk but which concerns the surface. A thermodynamic definition is given by Müller and Saúl [24] on the basis of an interfacial excess quantity. Choosing the z-axis as the normal of the surface, the surface stress tensor is symmetric and comprises only two nonzero components: σ_{xx} and σ_{yy}.

The Shuttleworth's equation links the surface stress component $\sigma_{ij}^{\text{surf}}$ with the surface energy γ

$$\sigma_{ij}^{\text{surf}} = \frac{1}{A}\frac{\partial(\gamma A)}{\partial \varepsilon_{ij}} = \gamma_0 \partial_{ij} + \frac{\partial \gamma}{\partial \varepsilon_{ij}} \tag{4.27}$$

where A is the surface area and γ_0 the surface energy of the initial surface (before the deformation).

The *local pressure*, in an atomistic model, represents the pressure localized on each atomic site. It corresponds to the trace of the stress tensor

$$P = -\frac{1}{3}\sum_i \sigma_{ij} \tag{4.28}$$

It derives from the energy of the system using the definition of the hydrostatic pressure as given by Kelires and Tersoff [25]:

$$P_i = -\frac{\mathrm{d}E_i}{\mathrm{d}\ln V_i} = -\frac{r_{ij}}{3}\frac{\mathrm{d}E_i}{\mathrm{d}r_{ij}} \tag{4.29}$$

where E_i is the energy of the system at site i, V_i is the atomic volume, and r_{ij} is the distance between the atom at site i and their neighbors j.

4.3 Relaxations in Surfaces and Interfaces

Surfaces and interfaces are the place of atomic relaxations because of the modification in the local environment of the atoms located at the surface (broken bonds) or at an interface (change in the nature and the distances of near neighbors). As a consequence, the surfaces and interfaces can reorganize their structure in order to minimize their energy, leading to surface reconstruction or interfacial dislocations.

We will consider in the following examples of surface reconstruction, surface with foreign adsorption (alloy surfaces), and heteroepitaxial thin films.

4.3.1
Surface Reconstructions

Because of the broken bonds at the surface, the interatomic distances of the surface atoms are modified as compared to the ones in the bulk. For example, it is well known that the metallic surfaces undergo an inward relaxation that is well reproduced by many-body potentials [26] at the difference of the pair potentials that give essentially an outward relaxation. Sometimes, the surface atoms can even reorganize their structure in order to minimize the surface energy. It is the case for the well-known gold(111) herringbone reconstruction [27, 28] as displayed by scanning tunneling microscopy (STM) pictures in Figure 4.3. Such reconstruction is well explained using a 2D Frenkel–Kontorova model by a spontaneous formation of stress domains including long-range elastic interactions [28].

We will concentrate here on another surface reconstruction, the (1×2) missing row reconstruction that concerns the (110) surface of the 5d transition metals. In the S. Olivier's thesis, directed by A. Saùl in Marseille [29], the author studied theoretically the influence of the stress on metallic surface reconstruction. The author first calculated in *ab initio* the surface energy gain to reconstruct the (1×2) (110) surface into the missing row (1×2) structure. The author found as illustrated in Figure 4.4 that only the 5 d Ir, Pt, and Au metals reconstruct ($\Delta\gamma < 0$) in good agreement with the experiments. Then, the author wanted to determine a criterion, beyond the energetic one that supposes to know the final reconstructed structure, in order to predict if the surface is susceptible or not to undergo the reconstruction. The author performed a detailed description of the surface stress tensor of the unreconstructed surface as compared to the reconstructed one. As mentioned before, the z

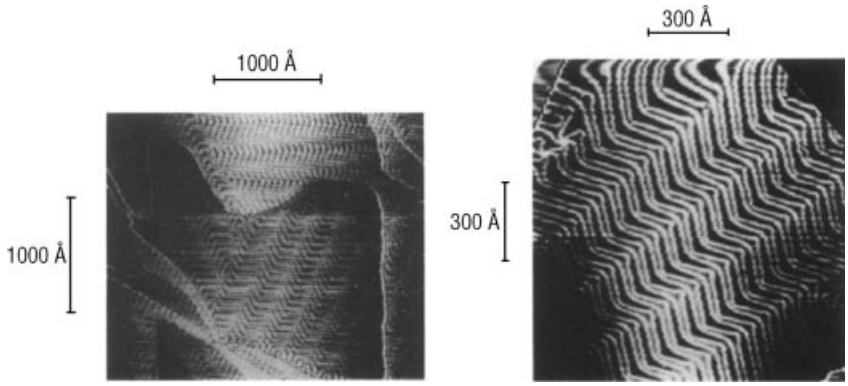

Figure 4.3 Figures reproduced from Barth *et al*. [27].

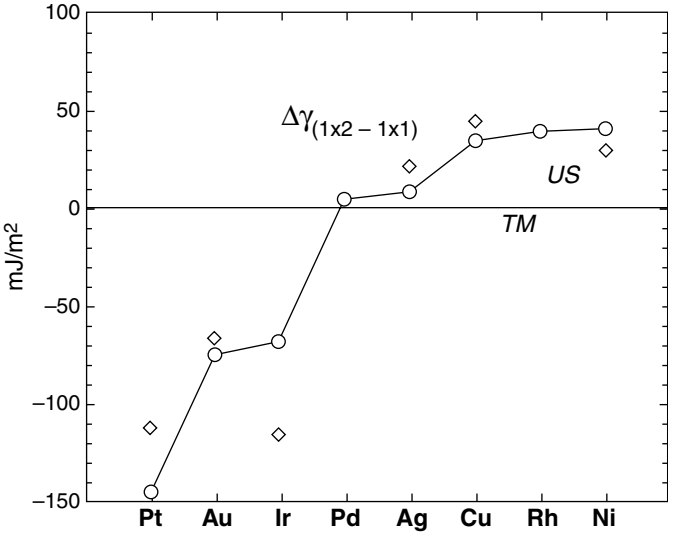

Figure 4.4 Surface energy difference between the (1 × 2) (110) reconstructed surface and the (1 × 1) (110) surface for the late-transition metals calculated using the density functional theory and the PWSCF (Plane-Wave Self-Consistent Field) code [30] with a slab of 12 atomic planes (diamonds) or a slab of 18 atomic planes (circles and continuous line). Reproduced from Ref. [29].

components are necessarily vanished by definition at the surface and there are only the σ_{xx} and σ_{yy} that are nonzero. Looking for a general criterion to separate the 3d and 4d metals (which do not reconstruct) from the 5d metals (which do reconstruct), the author first considered general tendencies as observed on other types of surfaces. For example, the Au(111) surface has the tendency to densify in the herringbone reconstruction, in order to compensate the lack of bonds. But this is clearly not the case here as the surface suppresses itself some rows leading to an even more open surface. Then, the author researched if the reconstruction was a way to release the surface stress as compared to the unreconstructed surface. The results show no clear difference in behavior between the 5d metals and the others, and even some possible increase in some surface stress components on the reconstructed surface. So, such criterion, which is not necessarily sufficient, but can be sufficient in some cases as we will see hereafter, is not a good criterion in that case. The best criterion the author obtained comes from the derivation of the surface energy as a function of the strain; in other words, the Shuttleworth equation as expressed before. In the graph of Figure 4.5, we see how the 5d metals are well separated from other transition metals, in order to discriminate the metals with tendency to reconstruct the (110) surface. Finally, it has also been checked that the driving force for this reconstruction comes from the electronic structure and in particular the relativistic effects in what concerns the 5d transition metals.

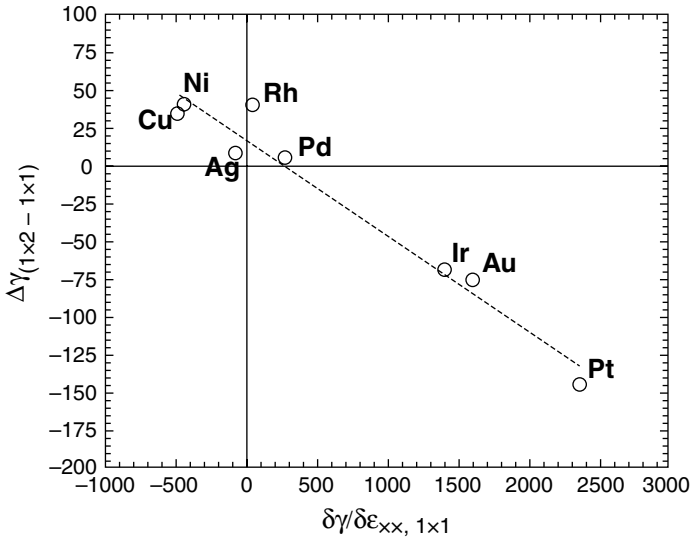

Figure 4.5 Same as Figure 4.4 for a slab of 18 atomic planes but plotted as a function of the derivative of the surface energy as a function of the deformation in the *x*-direction, in the unreconstructed (1×1) structure. Reproduced from Ref. [29].

4.3.2
Surface Alloys: a Simple Case of Heteroatomic Adsorption

The adsorption of Ag atoms on a surface of Cu(111) leads to interesting superstructures because of the strong size mismatch. The first modelization of an Ag monolayer deposited on Cu(111) substrate by quenched molecular dynamics simulation in the TB-SMA potential (as described in Section 1.1.2) showed that the system adopts a $p(10 \times 10)$ superstructure in good agreement with low-energy electron diffraction (LEED) experiments [31]. The atomistic simulations show beyond the periodicity an original motif with a strong corrugation of the surface layer extended in the substrate on the first 10 surface layers [32]. This corrugation is well illustrated by the local pressure map as depicted in Figure 4.6a and b, where the gray scale represents the pressure scale from tensile zones (in white) to black zones (in black). Such picture is directly comparable to the atomic elevation map of the Ag surface atoms (see Figure 4.7a) and the STM image [33] (Figure 4.7b). However, the STM images suggest other possible structures because of the bright atoms inside the dark triangles. Such STM picture is better represented with a structure where four or five atoms have been removed in the Cu layer in order to release the local pressure in compression to the Cu layer (Figure 4.6b without Cu vacancies: we observe black zones in compression that disappear with the introduction of Cu vacancies in Figure 4.6d).

In that case, the stress release by the introduction of Cu vacancies consisting in the formation of partial dislocation loops is a way not only to reduce the local pressure but

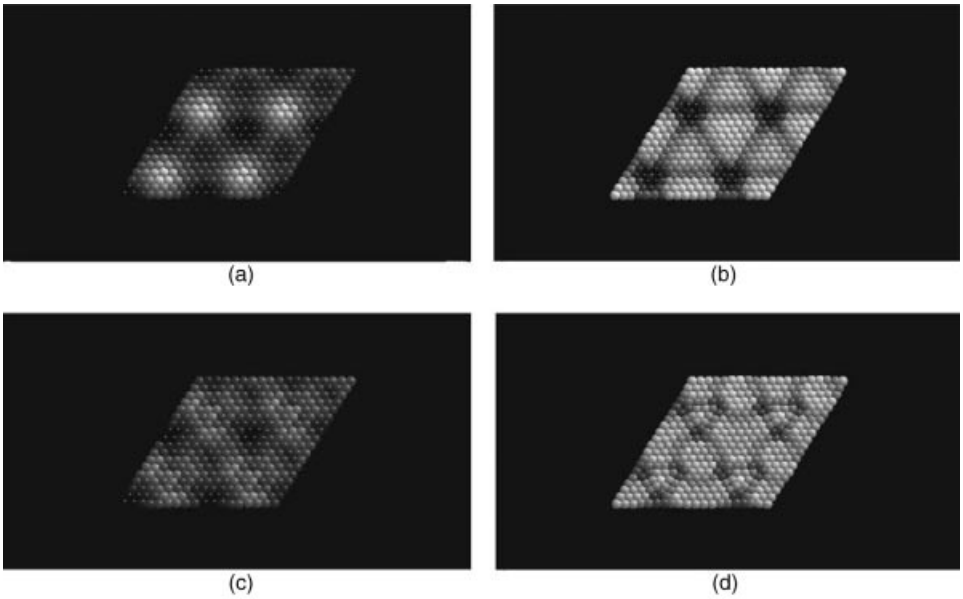

Figure 4.6 Local pressure maps in the Ag (a) and (c) and Cu (b) and (d), layers for the (10×10) superstructure of Ag/Cu(111), without (a) and (b) and with five Cu vacancies (c) and (d). The gray scale is chosen such that the white/black atoms are the most tensile/compressed ones with the following extreme values: In the Ag layer, $P_{min} = -88$ kbar and $P_{max} = 19$ kbar; and in the Cu layer $P_{min} = -77$ kbar and $P_{max} = 84$ kbar. Adapted from Ref. [32].

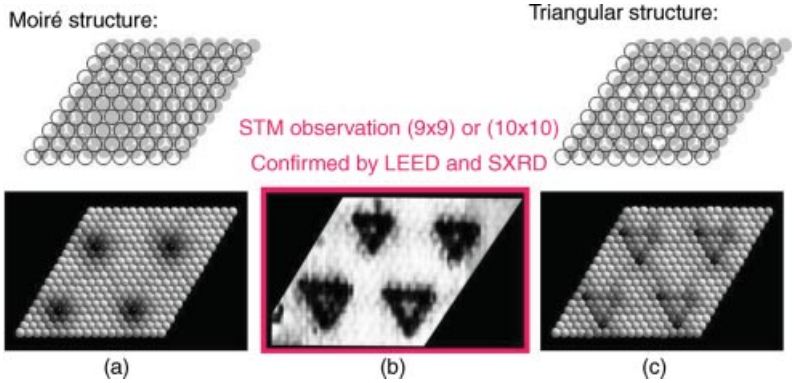

Figure 4.7 Height elevation maps in the Ag layer of the Ag/Cu(111) (10×10) superstructure (a) and with five vacancies (c). Black and white colors are associated with the deepest and highest elevations with the typical extreme values: $H_{min} = -0.033$ nm, and $M_{max} = 0.075$ nm; adapted from Ref. [32] In (b) we recall the STM image from Ref. [33].

also to minimize the surface energy leading to the stabilization of a new superstructure in perfect agreement with STM observations.

4.3.3 Heteroepitaxial Thin Films

The last example of extended surface and interface is taken from a thin metallic film epitaxially grown on a MgO(100) substrate. Obviously, we do not consider the growth mode but only the structure of the film in a state we will consider as an equilibrium state. Such system has been both experimentally [34, 35] and theoretically studied [36], and here again the confrontation of the two approaches is stimulating. In that case, we also compared the atomistic approach with the continuous elastic theory to see to which extent the analytical elastic theory can be used.

In that system, as previously, the size mismatch leads to a deformation of the deposit that prefers to rearrange by introducing interfacial dislocations in order to release the elastic deformation. The difference with the preceding case is that the MgO(100) substrate is rigid (an approximation of our model), which prevents any deformation (or even vacancy formation) in the substrate. However, because of the different nature of the two materials (a metal and an oxide), such hypothesis is legitimate in a first approximation, but we should go beyond in further studies using a new energetic model for the oxide and the metal–oxide interaction.

The metal is modeled within the TB-SMA as in the preceding case and the oxide is kept rigid, as mentioned above. The metal–oxide interaction is modeled via a potential energy surface approach fitted on *ab initio* calculations [37].

When considering a thin film of Ag on epitaxy on the MgO(100) substrate, the minimum energy structure corresponds to a partially relaxed film with interfacial dislocations, whose periodicity depends slightly on the film thickness. Figure 4.8 illustrates the propagation of the stress across a 20 monolayer (ML) film starting from the interface with the MgO(100) substrate where are located the core of the dislocations, up to the surface that we can see with a top view. We can distinguish the compressive zones in red and tensile zones in blue. Such motif at the surface is susceptible to change as a function of the film thickness, as shown in Figure 4.9, where thinner films display smaller motifs. In this figure, we also compare the stress profile using an elastic model and the atomistic model. In conclusion, we notice that the two models reach their best agreement for the thicker film (20 ML), where the elastic model is almost as precise as the atomistic model. For 7 and 5 ML, the agreement is still good, far from the dislocation core, but we clearly see that the elastic model fails to describe the stress on top of the dislocation core, which is not so surprising taking into account the approximations of the model.

Finally, let us mention the experimental study by grazing incidence small-angle X-ray scattering [34] that shows the self-organization of Co nanoparticles on a silver surface patterned by a buried dislocation network, which is a nice confirmation of what we have obtained in theory. Moreover, by calculating the adsorption energy of one Co atom on top of different sites on the nanostructured Ag surface, we show a clear correlation between the stress corrugation and the amplitude of the adsorption

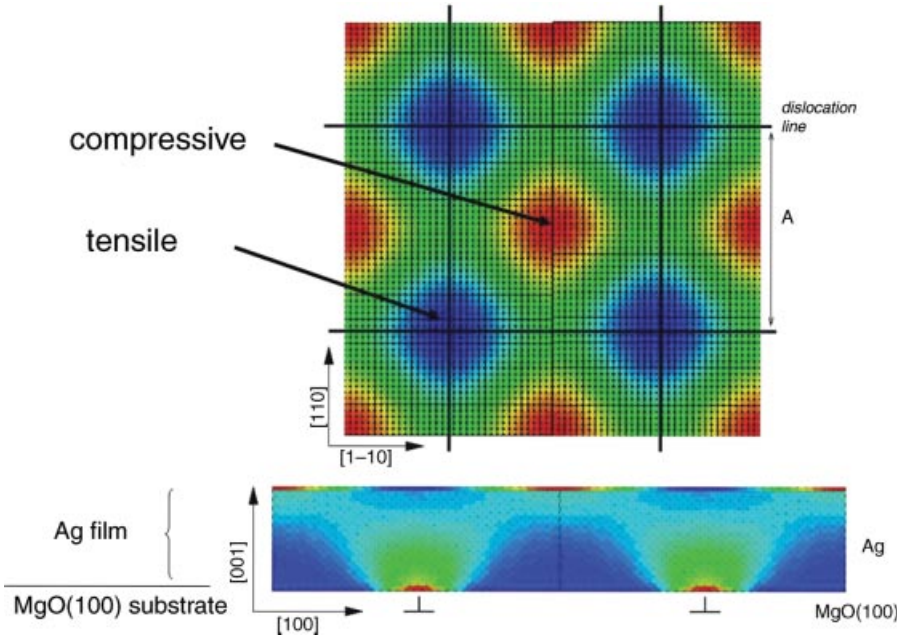

Figure 4.8 Top view and side view in the (010) plane of the atomic stress map of the Ag nanostructured film. Color code from red (dark) to blue (light) corresponds to compressive to tensile atomic sites. Because of its exponential decay, the stress field at the top surface is barely visible and, hence, a different color scale has been used. Adapted from Ref. [34].

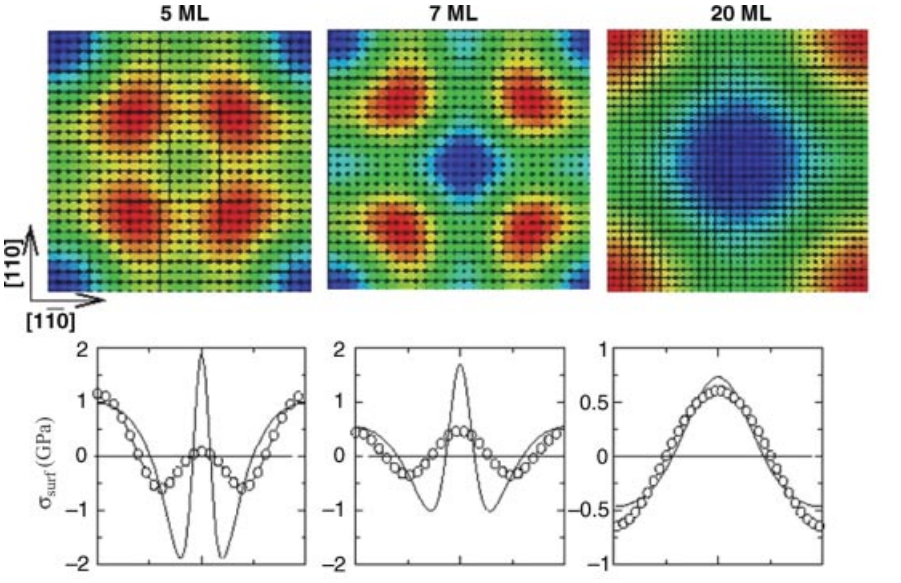

Figure 4.9 Top panel represents the map of the surface atomic stress (same color code as Figure 4.8) for different film thicknesses. Bottom panel gives the corresponding stress graph along the [100] direction ($x = y$). Circles for the atomistic calculations and full lines for the elastic theory calculations. Adapted from Ref. [36].

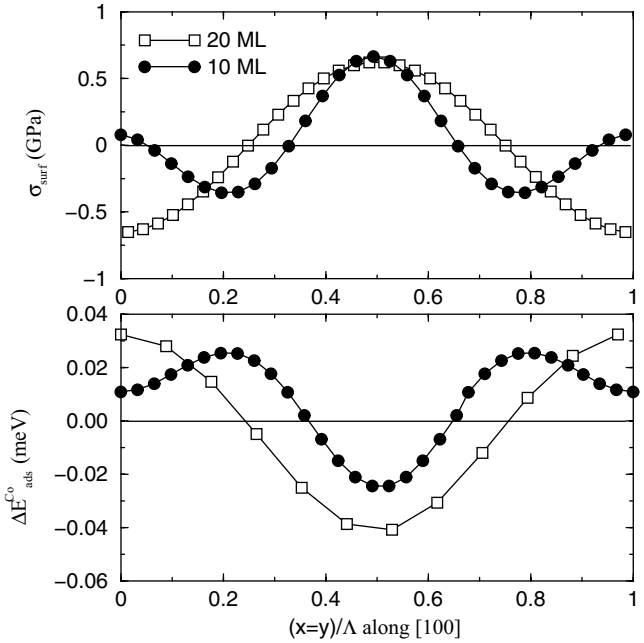

Figure 4.10 Surface atomic stress (top graph) and adsorption energy of a Co atom for different film thicknesses: 10 ML (circles) and 20 ML (squares) along the [100] direction ($x = y$). Λ is the length of the nanostructure.

energy (Figure 4.10), which is a good indication of the probable nucleation and growth of Co nanoparticles on it.

4.4
Relaxations in Nanoclusters

Because of their surface, nanoparticles undergo a surface stress in tension that is compensated by a core stress in compression leading to a total pressure equal to zero, as long as the nanoparticles are free from interaction with the exterior (under ultravacuum conditions). Their equilibrium shape respects the Wulff theorem up to quite small sizes if we include the edges and the corner energies in the Wulff description, as we have checked by comparing the results given by atomistic calculations and the thermodynamic approach [38]. As a function of their size, when the size becomes sufficiently small, they can change in structure in order to minimize the surface energy when the internal core pressure is not so high compared to the surface energy gain. The main result of the comparative study using thermodynamic and atomistic approach [38] is that not only edge effects but also mainly surface stress effects leading to a Laplace overpressure inside the particle have to be taken into account in order to validate the Wulff theorem for sizes smaller than 10 nm.

In the following, we will see the example of Pd-free nanoclusters and the possibility of stress release by vacancy introduction. As most of the nanoparticles are deposited on a support or included in a matrix, we will study the effect of the cluster environment on the structure and morphology of nanoparticles. We concentrate here on the case of metallic nanoparticles supported on a MgO(100) substrate. Finally, we will consider the alloy effect on bimetallic nanoclusters (called "nanoalloys") where the misfit between the two elements is at the origin of the stabilization of new structures that does not exist in pure systems.

4.4.1
Free Nanoclusters

It is well known that nanoparticles, and especially metallic nanoparticles, undertake new structures and notably the fivefold symmetry as their size decreases [39, 40]. This change in structure at small size results from an optimization of their surface by minimization of the surface energy forming only pseudo (111) facets in the icosahedral structure, whereas the fcc truncated octahedron, which is the optimized morphology taking into account the Wulff theorem, displays necessarily both (100) and (111) facets (see Figure 4.11). As the (111) facet is more dense, its surface energy is lower than more open (100) facet. However, the structural transformation from face-centered cubic (FCC) structure to fivefold symmetry structure is accompanied by an internal strain as illustrated in Figure 4.11. In this figure, the three morphologies are displayed with the two FCC ones and the icosahedron one. The first FCC structure

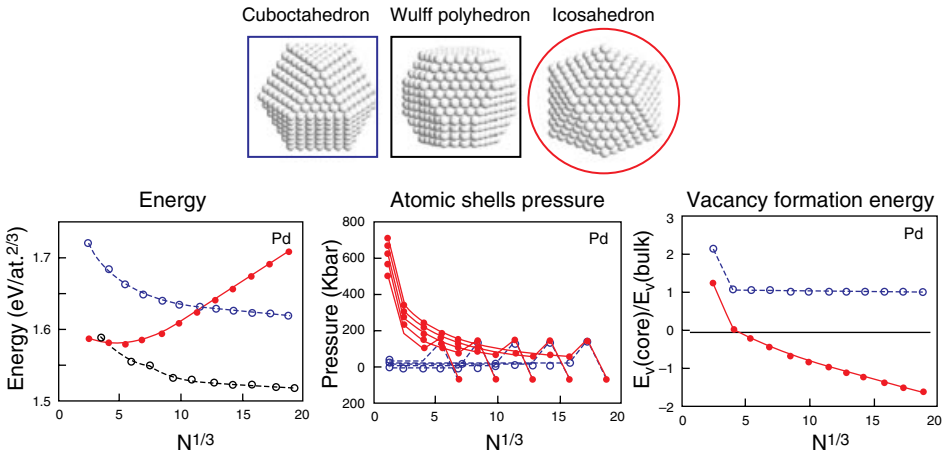

Figure 4.11 Energy, atomic shell pressure, and vacancy formation energy of Pd clusters under three different structures schematically represented: the cuboctahedron, the Wulff polyhedron, and the icosahedron. Their energy is compared with open blue circles for cuboctahedra, open black squares for the Wulff polyhedra, and red diamonds for icosahedra. The local pressure and vacancy formation energy are calculated for cuboctahedra and icosahedra only because they have exactly the same number of atoms to be compared.

is the cuboctahedron that has the same number of atoms as the icosahedron, each (100) facet is transformed in two (111) facets leading to 20 pseudo (111) facets in the icosahedral structure. This structure has six fivefold symmetry axis crossing two vertices. The second FCC structure is called the Wulff polyhedron because it optimizes the extension of the facets according to the Wulff construction that links the surface energy to the distance of the facet to the center of the particle. The extension of the (111) facets and the reduction of the (100) ones in the Wulff polyhedron compared to the cuboctahedron makes the Wulff polyhedron much more stable. The energy per cluster is reported in Figure 4.11 and we notice that the icosahedron is stable only at very small size. The critical size of transition from one structure to another is very sensitive to the metal itself and the icosahedron is stable on a larger range of size in Cu [40].

Looking at the local pressure on each concentric layer of the icosahedron as compared to the cuboctahedron (Figure 4.11), we clearly see that the icosahedron is highly compressed in its core whereas the equivalent cuboctahedron undergoes only a slight tension/compression at the vicinity of the surface, with an oscillating profile in order to cancel the total pressure. In order to attenuate the very high stress on the central site of the icosahedron, it is possible to remove the atom on the central site [41]. This leads to the next graph in Figure 4.11 where we see that the vacancy formation energy on the central site of the icosahedra can be negative for a size larger than 100 atoms, whereas with no surprise it is positive and equal to the bulk vacancy formation energy in the case of cuboctahedra.

4.4.2
Supported Nanoclusters

When the nanoclusters are in contact with a support, their structure is susceptible to be modified by their interaction with the substrate. This is the case of metallic clusters deposited on the MgO(100) surface. We first checked that the Wulff–Kaishew theorem that is an extension of the Wulff theorem but on supported systems (analogous to the Young–Dupré relation for a liquid droplet on a solid substrate) also works for nanoparticles. As for free clusters, this macroscopic thermodynamic approach can be extended to small sizes at the condition we integrate the variations in the adhesion energy with cluster size [42]. Indeed, the adhesion energy is one of the energetic ingredients in the Wulff–Kaishew equation where the ratio

$$\frac{\gamma_i}{h_i} = \frac{2\gamma_A - W}{H} \tag{4.30}$$

is a constant. γ_i and γ_A are the facet energy of facets i and A, A being the top facet; W is the adhesion energy, and H is the height of the particle. In the epitaxial relation with the MgO(100) substrate, due to the lattice mismatch of 8% between the Pd deposit and the MgO(100) surface, the Pd deposit is strained in order to accommodate the lattice of the substrate. The metal atoms have a preferential adsorption site on top of the oxygen atoms so that adhesion energy is optimal when the maximum of Pd atoms are adsorbed on top of oxygen atoms (as illustrated in Figure 4.12). As a consequence,

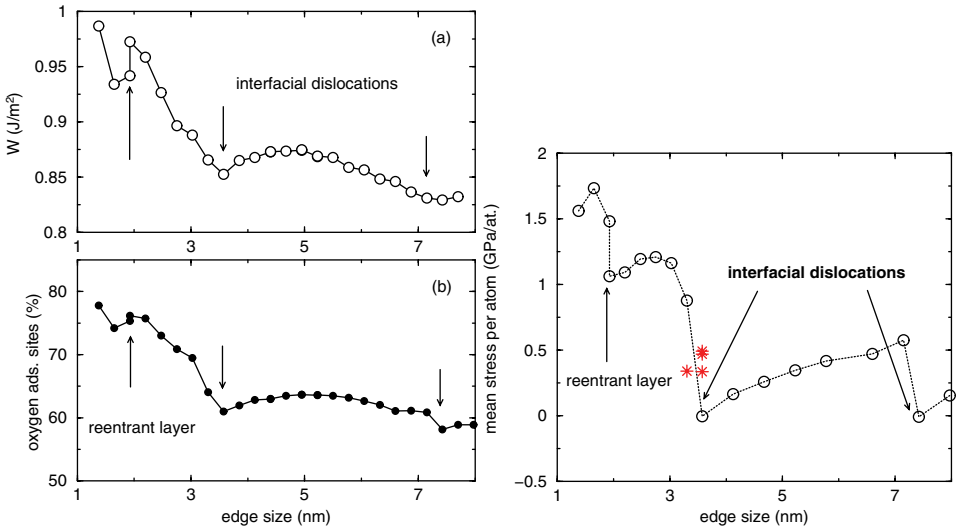

Figure 4.12 Adhesion energy (W), percentage of metal atoms adsorbed on top of oxygen sites, and average stress per atom and per particle as a function of cluster size. Adapted from Ref. [43].

the nanoparticle is highly stressed, as shown in Figure 4.12 where we can follow the total stress per atom and per particle as a function of the cluster size. This stress is fully relaxed by the introduction of the first interfacial dislocation, which corresponds to a Vernier rule between the relaxed nanoparticle and the substrate. Before the introduction of the second dislocation, the cluster is partially relaxed.

Such interfacial dislocations have been evidenced in Ni nanoparticles on MgO (100) surface by high-resolution electron microscopy [44].

4.4.3
Nanoalloys

Nanoalloys are typically systems referring to bulk alloys but with a finite size on the order of one to a few nanometers scale. As in the surface alloys mentioned in the previous section, the misfit between the two elements induces some strain and stress that are interesting to analyze in order to understand the kind of structure adopted by the system. In very small nanoalloys, we found a strong relation between the structure and the misfit that leads to the formation of what we have called "new magic polyicosahedral core–shell clusters" [45]. The term "magic" is generally attributed to highly stable structures. It is concerned first with the simple metal clusters with magic number of atoms corresponding to the completion of electronic shells. Then, more generally, it is concerned with the geometrical completion of atomic layers at the surface. Here, we propose a new criterion related to the composition of the bimetallic cluster. Indeed, in the particular cases of fivefold symmetry structures that are stabilized at small sizes, it is possible to release partially the internal stress by

replacing the core atoms by smaller atoms. They form core–shell structures with polyicosahedral symmetry (see Figure 4.13). These nanoalloys present a particularly high stability, related not only to their low energy compared to others but also to their high melting point compared to pure clusters of equivalent sizes [45]. Beside the stress relaxation, the driving forces responsible of such structures are the same as the ones leading to surface segregation and core/shell structures in nanoparticles that are the surface segregation of one of the elements (Ag in case of Ag–Cu and Ag–Ni) and the tendency to phase separation in bulk alloys.

Stress relief can have also surprising effects on the melting behavior of nanoalloys. It is illustrated by the single impurity effect on the melting of nanoclusters [46]. The lattice mismatch between the impurity and its matrix seems to play a decisive role in the melting property of a 55-atom icosahedron of Ag as illustrated below. When the lattice parameter of the impurity is the same as the Ag one, the melting behavior is the same as the pure Ag cluster. The melting temperature is shifted toward higher temperature when the lattice parameter of the impurity is smaller than the one of Ag, and the amplitude of the shift is well correlated with the lattice misfit (see Figure 4.14). Even if the relation between the stress and the thermodynamic stability is not trivial to

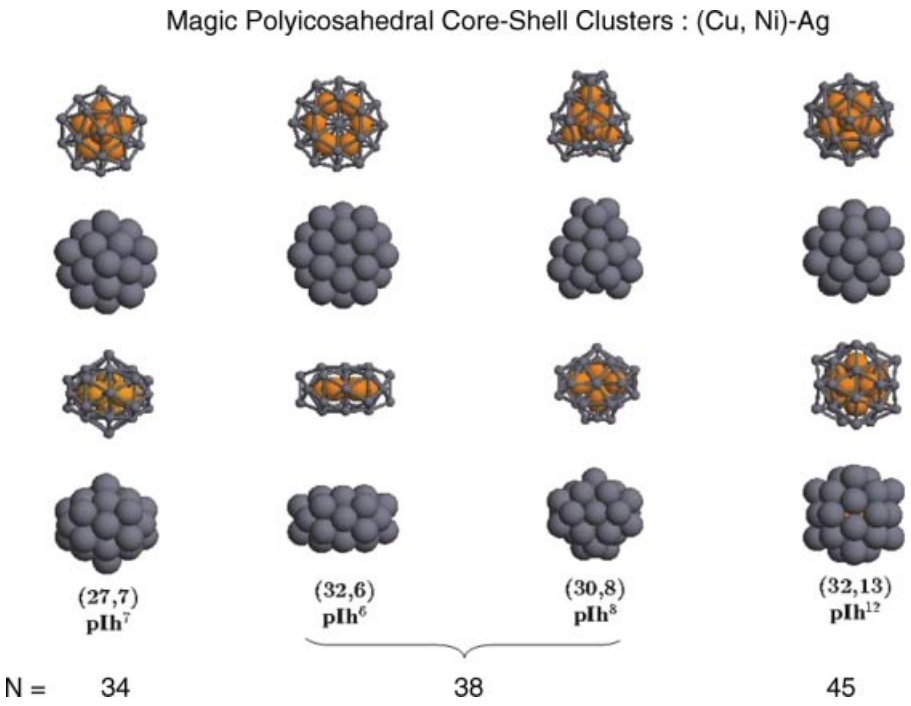

Figure 4.13 Different views of magic core–shell polyicosahedra with Cu or Ni atoms in the core (yellow color) and Ag atoms on the shell (gray color) with different sizes and compositions. Adapted from Ref. [45].

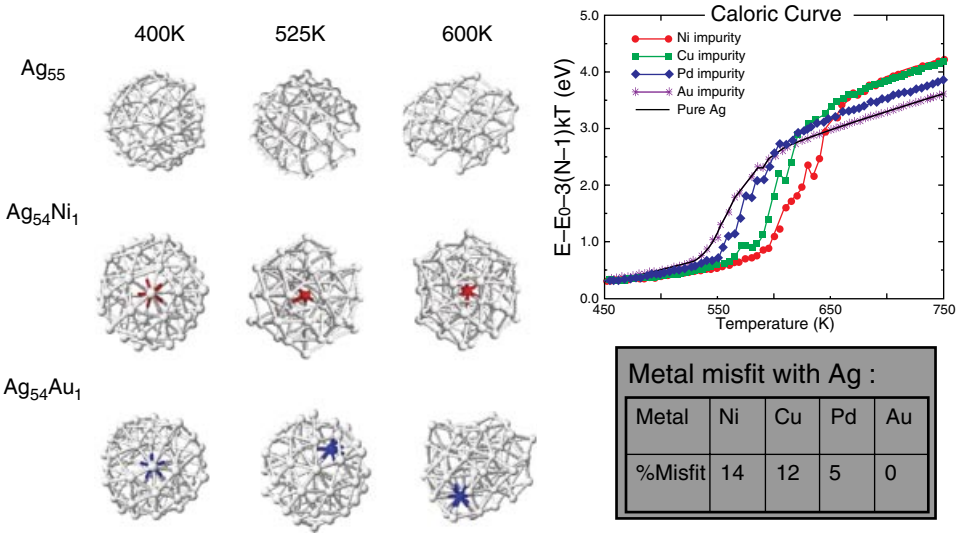

Metal misfit with Ag :

Metal	Ni	Cu	Pd	Au
%Misfit	14	12	5	0

Figure 4.14 Representation of pure 55 atoms Ag icosahedra at different temperatures and the same with an impurity of Ni or Au. While the pure and Au-doped clusters melt at 600 K, the Ni-doped one is still solid at this temperature. Besides, the caloric curves relative to different impurities in this cluster are plotted and a correlation is made between the melting transition and the lattice parameter mismatch. Adapted from Ref. [46].

characterize, this is an evidence of the implication of the stress release in the higher stability of nanoclusters.

4.5 Conclusions

The potentiality of the atomistic simulations in the description and analysis of the strain and stress of a nanoscale system is promising, in particular the analysis of their possible relaxations at the atomic scale in unsolicited systems. Such systems that are free of external stress present nevertheless local or extended defects compared to the bulk solid giving rise to quite complex atomic structures, as we have seen in the different examples presented here. This opens up a wide domain of research in what concerns systems under external stress. Many questions arise when considering mechanical properties at the nanoscale because the points of the contact are already a vast domain to be investigated. We can think about the experiments performed using an STM tip touching the surface and, by a slow backward movement, being able to form a quasiatomic metallic wire of gold or platinum. Possessing interesting transport properties with the quantization of the current, the mechanical properties of these metallic nanowires should also be interesting, as an extreme case of the well-known nanopillars. However, the difference in size, from one nanometer or less in

one case to some tens or hundreds of nanometers in the other case makes the atomistic description not always appropriate in all the situations. This is why it is necessary to have a constant feedback to the macroscopic thermodynamic description (notably in terms of the elastic theory) in order to validate or extrapolate if possible the results of the atomistic modelization.

References

1 Hamers, R.J., Tromp, R.M., and Demuth, J.E. (1986) Surface electronic structure of si(111)-(7 × 7) resolved in real space. *Phys. Rev. Lett.*, **56**, 1972–1975.

2 Barth, J.V., Brune, H., Ertl, G., and Behm, R.J. (1990) Scanning tunneling microscopy observations on the reconstructed au(111) surface: atomic structure, long-range superstructure, rotational domains, and surface defects. *Phys. Rev. B*, **42**, 9307–9318.

3 Hohenberg, P. and Kohn, W. (1964) Inhomogeneous electron gas. *Phys. Rev.*, **136**, B864–B871.

4 Kohn, W. and Sham, L.J. (1965) Self-consistent equations including exchange and correlation effects. *Phys. Rev.*, **140**, A1133–A1138.

5 Friedel, J. (1969) in *The Physics of Metals* (ed. J.M. Ziman), Cambridge University Press, Cambridge, p. 340.

6 Rosato, V., Guillopé, M., and Legrand, B. (1989) Thermodynamical and structural properties of f.c.c. transition metals using a simple tight-binding model. *Phil. Mag. A*, **59**, 321.

7 Simmons, G. and Wang, H. (1971) *Single Crystal Elastic Constants and Calculated Aggregated Properties: A Handbook Second Edition*, MIT Press.

8 Foiles, S.M., Baskes, M.I., and Daw, M.S. (1986) Embedded-atom-method functions for the fcc metals Cu, Ag, Au, Ni, Pd, Pt, and their alloys. *Phys. Rev. B*, **33**, 7983–7991.

9 Jacobsen, K.W., Norskov, J.K., and Puska, M.J. (1987) Interatomic interactions in the effective-medium theory. *Phys. Rev. B*, **35**, 7423–7442.

10 Stave, M.S., Sanders, D.E., Reaker, T.J., and DePristo, A.E. (1990) Corrected effective medium method. V. Simplifications for molecular dynamics and Monte Carlo simulations. *J. Chem. Phys.*, **93**, 4413–4427.

11 Methfessel, M., Hennig, D., and Scheffler, M. (1992) Trends of the surface relaxations, surface energies, and work functions of the 4d transition metals. *Phys. Rev. B*, **46**, 4816–4829.

12 Skriver, H.L. and Rosengaard, N.M. (1992) Surface energy and work function of elemental metals. *Phys. Rev. B*, **46**, 7157–7168.

13 Guillopé, M. and Legrand, B. (1989) (110) Surface stability in noble metals. *Surf. Sci.*, **215**, 577–595.

14 Frenkel, D. and Smit, B. (1996) *Understanding Molecular Simulation: From Algorithms to Applications*, Academic Press.

15 Allen, M.P. and Tildesley, D.J. (1987) *Computer Simulations of Liquids*, Oxford Science Publications.

16 Voter, A.F. (1997.) Hyperdynamics: accelerated molecular dynamics of infrequent events. *Phys. Rev. Lett.*, **78**, 3908–3911.

17 Barkema, G.T. and Mousseau, N. (1996) Event-based relaxation of continuous disordered systems. *Phys. Rev. Lett.*, **77**, 4358–4361.

18 Jonsson, H., Mills, G., and Jacobsen, K.W. (1998) Nudged elastic band method for finding minimum energy paths of transitions, in *Classical and Quantum Dynamics in Condensed Phase Simulations* (eds B.J. Berne, G. Ciccotti, and D.F. Coker), World Scientific, p. 385.

19 Henkelman, G. and Jonsson, H. (1999) A dimer method for finding saddle points on high dimensional potential surfaces using only first derivatives. *J. Chem. Phys.*, **111**, 7010.

20 Wales, D.J. (2003) *Energy Landscapes*, Cambridge University Press.

21 Ferrando, R., Fortunelli, A., and Johnston, R.L. (2008) Searching for the optimum structures of alloy nanoclusters. *Phys. Chem. Chem. Phys.*, **10**, 640.

22 Verlet, L. (1967) Computer "experiments" on classical fluids. I. Thermodynamical properties of Lennard–Jones molecules. *Phys. Rev*, **159**, 98.

23 Metropolis, N., Metropolis, A.W., Rosenbluth, M.N., Teller, A.H., and Teller, E. (1953) Equation of state calculations by fast computing machines. *J. Chem. Phys.*, **21**, 1087.

24 Müller, P. and Saúl, A. (2004) Elastic effects on surface physics. *Surf. Sci. Rep.*, **54**, 157–258.

25 Kelires, P.C. and Tersoff, J. (1989) Equilibrium alloy properties by direct simulation: oscillatory segregation at the Si–Ge(100) surface. *Phys. Rev. Lett.*, **63** (11), 1164–1167.

26 Desjonquères, M.C. and Spanjaard, D. (1996) *Concepts in Surface Physics*, 2nd edn, Springer, Berlin.

27 Barth, J.V., Brune, H., Ertl, G., and Behm, R.J. (1990) Scanning tunneling microscopy observations on the reconstructed au(111) surface: atomic structure, long-range superstructure, rotational domains, and surface defects. *Phys. Rev. B*, **42**, 9307–9318.

28 Narasimhan, S. and Vanderbilt, D. (1992) Elastic stress domains and the herringbone reconstruction on au(111). *Phys. Rev. Lett.*, **69**, 1564–1567.

29 Olivier, S. (2004) Rôle des Contraintes Dans les Reconstructions de Surfaces Métalliques. PhD thesis, Université de la Méditerranée, Faculté des Sciences de Luminy, Marseille.

30 Baroni, S., Corso, A.D., de Gironcoli, S., and Giannozzi, P, http://www.pwscf.org.

31 Bauer, E. (1967) Multiple scattering versus superstructures in low energy electron diffraction. *Surf. Sci.*, **7**, 351–364.

32 Meunier, I., Tréglia, G., Gay, J.M., Aufray, B., and Legrand, B. (1999) Ag/cu (111) structure revisited through an extended mechanism for stress relaxation. *Phys. Rev. B*, **59**, 10910–10917.

33 Aufray, B., Gothelid, M., Gay, J.M., Mottet, C., Landmark, E. *et al.* (1997) Ag/cu(111): incommensurate reconstruction studied with STM and surface X-ray diffraction. *Microanal. Microstruct.*, **8**, 167–174.

34 Leroy, F., Renaud, G., Letoublon, A., Lazzari, R., Mottet, C., and Goniakowski, J. (2005) Self-organized growth of nanoparticles on a surface patterned by a buried dislocation network. *Phys. Rev. Lett.*, **95**, 185501.

35 Robach, O., Renaud, G., and Barbier, A. (1999) Structure and morphology of the Ag/MgO(001) interface during *in situ* growth at room temperature. *Phys. Rev. B*, **60**, 5858–5871.

36 Ouahab, A., Mottet, C., and Goniakowski, J. (2005) Atomistic simulation of Ag thin films on MgO(100) substrate: a template substrate for heterogeneous adsorption. *Phys. Rev. B*, **72**, 035421.

37 Vervisch, W., Mottet, C., and Goniakowski, J. (2002) Theoretical study of the atomic structure of Pd nanoclusters deposited on a MgO(100) surface. *Phys. Rev. B*, **65**, 245411.

38 Müller, P. and Mottet, C. (2007) Equilibrium nanoshapes: from thermodynamics to atomistic simulations. *J. Comput. Theor. Nanosci.*, **4**, 316–325.

39 Baletto, F. and Ferrando, R. (2005) Structural properties of nanoclusters: energetics, thermodynamics, and kinetic effects. *Rev. Mod. Phys.*, **77**, 371–424.

40 Baletto, F., Ferrando, R., Fortunelli, A., Montalenti, F., and Mottet, C. (2002) Crossover among structural motifs in transition and noble-metal clusters. *J. Chem. Phys.*, **116**, 3856–3863.

41 Mottet, C., Tréglia, G., and Legrand, B. (1997) New magic numbers in metallic clusters: an unexpected metal dependence. *Surf. Sci.*, **383**, L719–L727.

42 Mottet, C. and Goniakowski, J. (2007) Influence of epitaxial strain on supported metal cluster shapes via atomistic simulations. *J. Comput. Theor. Nanosci.*, **4**, 326–334.

43 Vervisch, W., Mottet, C., and Goniakowski, J. (2003) Effect of epitaxial strain on the atomic structure of Pd clusters on MgO(100) substrate. *Eur. Phys. J. D*, **24**, 311–314.

44 Sao-Joao, S., Giorgio, S., Mottet, C., Goniakowski, J., and Henry, C.R. (2006) Interface structure of Ni nanoparticles on MgO (100): a combined HRTEM and molecular dynamic study. *Surf. Sci.*, **600**, L86–L90.

45 Rossi, G., Rapallo, A., Mottet, C., Fortunelli, A., Baletto, F., and Ferrando, R. (2004) Magic polyicosahedral core–shell clusters. *Phys. Rev. Lett.*, **93**, 105503.

46 Mottet, C., Rossi, G., Baletto, F., and Ferrando, R. (2005) Single impurity effect on the melting of nanoclusters. *Phys. Rev. Lett.*, **95**, 035501.